Chemical Engineering Science 184 (2018) 62–71

Contents lists available at ScienceDirect

Chemical Engineering Science

journal homepage: www.elsevier.com/locate/ces

Molecular dynamics simulation of the aggregation phenomenon in the late stages of silica materials preparation

Reza Gholizadeh, Yujun Wang *

State Key Laboratory of Chemical Engineering, Department of Chemical Engineering, Tsinghua University, Beijing 100084, China

HIGHLIGHTS

- Dreiding force field was used in whole calculations.
- Investigations conducted using the Forcite and Amorphous cell modules.
- Diameters of the generated aggregates and pores increased.
- The number of "aggregates and pores" first increased and then decreased.
- The volume of pores first increased and then decreased with the reaction proceeding.

GRAPHICAL ABSTRACT

Two stability and aggregation phenomena at the early and late stages of silica materials preparation occur, respectively.

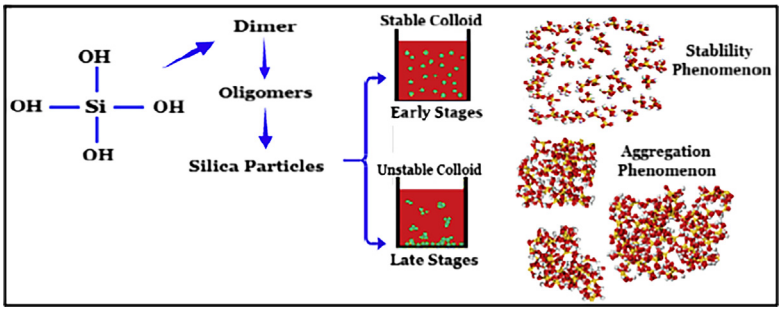

ARTICLE INFO

Article history:
Received 6 July 2017
Received in revised form 12 March 2018
Accepted 24 March 2018
Available online 27 March 2018

Keywords:
MD simulation
Aggregation
Silicic acid monomer
Lennard–Jones potential
Force field

ABSTRACT

Molecular dynamics simulations are employed to investigate the aggregation behavior at the late stages of silica production in a colloidal solution to find new insights into the structures and dynamics of the produced aggregates and pores. The implemented theoretical investigations used the Amorphous cell and Forcite modules, and Dreiding force field of Materials Studio package. The key thermodynamic parameters, mean squared displacements, and radial distribution functions were calculated. Results revealed that aggregation occurred in the late stages due to the negative value of Gibbs free energy. Diameters of the generated "aggregates and pores" continuously increased while the number of "aggregates and pores" first increased and then decreased. Furthermore, the volume of pores first rose and then fell as the reaction proceeded. Variations of reactant numbers had the noticeable influence on the pores and aggregates topologies. The number of aggregates and pores had an upward trend while their diameters slightly reduced when more effective molecules were involved in the aggregation process. In addition, the shape of the aggregates examined and found that the predominant shapes of the aggregates were spherical.

1. Introduction

The aggregation process of nanoparticles is an interesting research field in a variety of subjects such as precipitation, sediment formation, crystallization, liquid-solid separation, microbe, and cell growth. A large amount of research has been conducted in the field of silica materials production through experimentation and theoretical examination in the past few decades. The main motivation of these efforts is enormous applications of silica materials in different fields such as electronic devices, food and pharmaceutical industries for biosensors (Jurkić et al., 2013; Sharma and

* Corresponding author.
E-mail address: wangyujun@mail.tsinghua.edu.cn (Y. Wang).

https://doi.org/10.1016/j.ces.2018.03.045
0009-2509/

Trout, 2015), enzyme supporters (Ogorzalek et al., 2015) and controlled drug release and delivery (Aydin et al., 2016; Guo et al., 2007).

Furthermore, research and experiments reveal that silica materials have unique catalytic properties due to the differences between their specific structures from the bulk. Currently, silica materials are produced through experiments using different techniques such as sol-gel, gas-phase chemical reaction, precipitation, etc. (Chou et al., 2014; Patel et al., 2007; Sun and Rigby, 1997). It was found that the precipitation method is more economical and thus favorable. The particles attach to each other to form aggregates in a destabilized colloidal solution while being distributed separately in a stable colloidal solution. Many studies have been carried out to explore the configurations of the destabilized colloidal solutions, kinetics and to explore the effects of factors such as solution chemistry on aggregation phenomenon (Jenkins et al., 2008, 2009; Vold, 1982). A large part of the research work regarding the aggregation process was carried out on clusters of nanoparticles (Li et al., 2010, 2012). Studies and theoretical investigations on the aggregation processes of small nanoparticles (particle diameters less than 10 nm, especially in the 2–3 nm range) in a colloidal solution can be advantageous to the understanding of scale effect, interfacial structure and interactions between particle–particle and particle–solvent. Evaluation of nanoparticle movement needs a comprehensive understanding of mutual forces between nanoparticles including the van der Waals attractions, Born repulsions, and electrostatic interactions (Delay and Frimmel, 2012). The van der Waals attractive forces between particles can be computed through the Hamaker approach (Hamaker, 1937), Lifshitz's continuum theory (Dzyaloshinskii et al., 1961; Pashley, 1981), or Derjaguin-Muller–Toporov (DMT)'s approximation (Schiller et al., 2011). Computer molecular dynamics simulations support scientists to overcome the difficulties of experimentations. These computational research works have an obvious role in the evaluations of material properties and make research work more efficient. As well, understanding of processes in the atomistic level is possible only using computer simulations. Several investigations have been carried out using molecular dynamics simulations to explore the microstructure of silica nanoparticles in colloidal solutions. Van Hoang studied the structural properties of silica nanoparticles via Radial Distribution Function (RDF), mean squared displacement (MSD), coordination numbers, and bond-angle distributions through molecular dynamics simulations (Hoang, 2007). Sun et al. calculated normal contact and non-contact forces between two silica nanoparticles in a Lennard-Jones liquid using MD simulations (Sun et al., 2013a). Gompper et al. analyzed a mesoscale simulation method which is called multi-particle collision dynamics or stochastic rotation dynamics. The method consists of alternating streaming and collision steps in an ensemble of point particles (Gompper et al., 2012).

In the past decade, theoretical investigations have been developed for property calculations in a wide range of length and timescales, ab-initio studies of nucleation (Pereira et al., 1997, 1998) and stability of oligomers (He et al., 2006; Pereira et al., 1999), molecular dynamics using reactive potentials (Rao and Gelb, 2004; Yamahara and Okazaki, 1998). Lu et al. investigated the aggregation process of TiO_2 nanoparticles in water. Their results showed that the aggregation of nanoparticles in colloidal solutions influenced by particle size (Lu et al., 2015). Sun et al. investigated interaction forces between two silica nanoparticles via molecular dynamics (MD) simulations and their results compared with Hamaker approach. They found Coulomb's law is valid for the calculation of electrostatic potential (Sun et al., 2013b). Our laboratory synthesized silica nanoparticles through a novel process using the combination of a micro-reactor and a stirred-tank reactor for the controlled preparation of silica materials with a large pore volume and narrow-pore-diameter distribution. The innovation method of the above mentioned preparation is that it used a unique membrane dispersion microreactor (Wang et al., 2016, 2010; Zhang et al., 2016). The silica productionreaction is described as Eq. (1)

$$Na_2SiO_3 + H_2SO_4 \rightarrow SiO_2 + H_2O + Na_2SO_4 \quad (1)$$

Dimer and cyclic are produced from silicic acid monomers through condensation when the dispersed fluid (H_2SO_4) and the continuous fluid (Na_2SiO_3) solutions come into contact as reactants at 70 °C. Dimer and cyclic polymers form in the early stages of SiO_2 production and are stable for an extended period of time if the concentration is less than 100 ppm SiO_2 (Iler, 1979). The silicic acid species grow and the nucleus appears. The nuclei further grow until aggregation and gelling happen to form silica gels. Before aggregation and gelation processes nuclei are in the stable the conditions. The gels disperse in a solvent after aging and washing due to spray drying. Microstructure in the membrane dispersion reactor determines the mixing time. Homogeneous super-saturation is achievable due to excellent mass transfer efficiency and therefore, the size distribution of the nanoparticles is controllable (Sun et al., 2013b). The pH value of the silica suspension is recorded to be 8.4 (Du et al., 2011; Wang et al., 2016; Zhang et al., 2016). The morphology of silica nanoparticles is shown in Fig. 1. This figure shows the process of silica nanoparticles production starting from monomer to large particles which is presented schematically by Iler (1979). This applies to aqueous systems, in which silica is somewhat soluble.

The main purpose of this research is the observation of the silicic acid monomers aggregations, trajectory information of silicic acid and sodium sulfate and water molecules in the studied colloidal solution. Atomistic trajectories, nanoparticles activities, diameters and numbers of aggregates and pores, and volume of pores are explored to describe these parameters. The main motivations to carry out this research were the enormous applications, the complexity, the limitations of experimental methods and the lack of knowledge about the mechanisms of aggregation phenomena of the silicic acid monomers. To the best of our knowledge, many studies carried out on aggregation of relatively large nanoparticles, in the 5–10 nm range, while there are only a few investigations of aggregation of small nanoparticles such as silicic acid in the monomer, dimer, cyclic and particle forms (Gompper et al., 2012; Sun et al., 2013a). Therefore, this research work is the one of promising research work on aggregation of the silicic acid nanoparticle. MD simulations were carried out using dreiding force field, amorphous cell and forcite modules of Materials Studio code.

2. Brief description of the DLVO theory

It is well-known that nanoparticles can self-assemble into large aggregates through internal and external forces (Giannini et al., 2011; Grzelczak et al., 2010; Hu et al., 2008). Understanding how interparticle interaction forces affect the construction and organization of nanoparticles is of importance to rationally design a detection method based on these nanoparticles. For charged nanoparticles, the classical Derjaguin–Landau–Verwey–Overbeek (DLVO) theory has been developed to study the net interaction (V_{net}) between particles in a colloidal solution. When two nanoparticles are close to each other in solution, the main contributions to the interaction energy come from the van der Waals attraction force (normally London forces and attractive in homo and hetero aggregations) and the repulsive interactions (V_R) from the overlap between the electrical double layers (normally repulsive in home

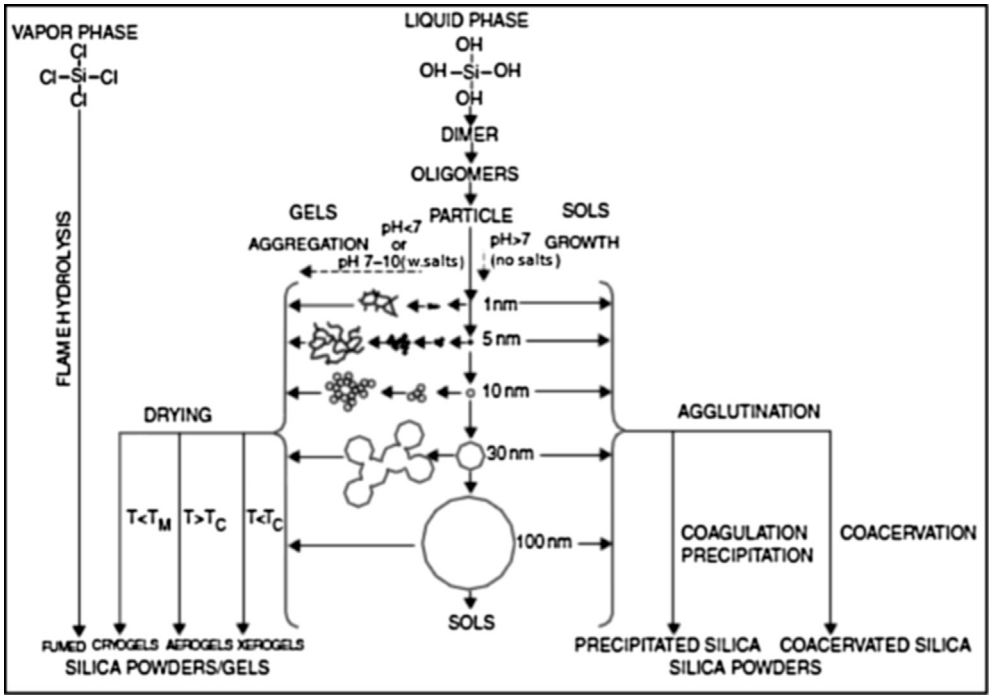

Fig. 1. Morphology of $Si(OH)_4$ nanoparticles (polymerization and aggregation of silicic acid monomers).

aggregation while attractive, repulsive or both in hetero aggregation) as Eq. (2) (Hunter, 1987):

$$V_{net} = V_{vdW} + V_R \tag{2}$$

V_{vdW} is defined as Eq. (3):

$$V_{vdW} = -\frac{A_H}{6}\left\{\frac{2a^2}{D^2+4Da} + \frac{2a^2}{(D+2a)^2} + \ln\left(1-\left(\frac{2a}{D+2a}\right)^2\right)\right\} \tag{3}$$

where A_H is the Hamaker constant (Kirk et al., 2011).

V_R can be defined in two forms as Eqs. (4) and (5) (Hu et al., 2013):

$$V_R = 2\pi\varepsilon_s\varepsilon_0 a\Psi^2 \ln\{1+e^{-kD}\} \quad \text{if } ka > 5 \tag{4}$$

$$V_R = 2\pi\varepsilon_s\varepsilon_0 a\Psi^2 e^{-kD} \quad \text{if } ka < 5 \tag{5}$$

where $\varepsilon_s, \varepsilon_0, a, \Psi, k, D$ are the relative dielectric constant of the solvent, the dielectric constant of the vacuum, the radius of the nanoparticles, the surface potential of the nanoparticles, the inverse Debye length and the distance of the closest nanoparticles, respectively. The presented Eqs. (2)–(5) are the principle equations of describing the aggregation phenomenon in the colloidal solutions. Milling et al. studied the effect of the medium on the vdW forces between Au spheres and a polytetrafluoroethylene surface. The interaction was repulsive in low polarity solvents which corresponded to a negative composite Hamaker constant (Milling et al., 1996). Yang et al. show the aggregation of AuNPs in sodium citrate aqueous solution is directed by electrostatic interactions (Yang et al., 2007). They developed a simple technique to fabricate linear chainlike aggregates of AuNPs. Kim et al. indicated that the experimental results of AuNP aggregation describable by the model in which interparticle interactions are defined by the classical DLVO theory (Kim et al., 2008).

3. Computational details

3.1. Configuration of the initial simulation system

A model system, which contained the silicic acid, sodium sulfate, and water molecules, was used to investigate the diffusion-limited aggregation process in the studied colloidal solution. All structures that are involved in the aggregation process were optimized before construction of the initial simulation box to find the lowest energy (Fig. 2). Further detailed information can be found in Table 1. The amorphous cell module of Accelrys Materials Studio package, San Diego, CA (Yu, 2014), was used in order to construct the initial simulation box. The simulation box contains 500Si $(OH)_4$, 500 Na_2SO_4 and 500 H_2O molecules. These numbers of molecules are found by comparing different numbers of silicic acid, sodium sulfate, and water molecules in order to make the MD simulations reliable, reasonable and accurate. In addition, finding the right numbers of molecules inside the simulation box has a significant effect on the reducing calculation time and amount. This constructed system is large enough to obtain sufficient information about the growth and aggregation processes of silicic acid monomers up to a few nanometers. The construction algorithm resembles that of a polymerization process, where molecules are "grown" into an empty box fragment by fragment. A fragment corresponds to the substructure of atoms between two rotatable bonds. Amorphous Cell automatically detects rotatable bonds along the backbone of the input model. Alternatively, you can specify the rotatable bonds by assigning torsion monitors to those bonds. In adding a next fragment, the algorithm probes a number of potential placements. The energy of each placement is evaluated from which the probability of each placement is calculated. Based on the probabilities, one of the candidates is selected, and the fragment is given its final placement.

Each silicic acid monomer has one silicon, four oxygen and four hydrogen atoms and four single type of Si—OH bonds. The constructed 3D Triclinic system along the X, Y, Z directions was orthorhombic, $60 \times 60 \times 60$ Å, $\alpha = \beta = \gamma = 90°$. The target density

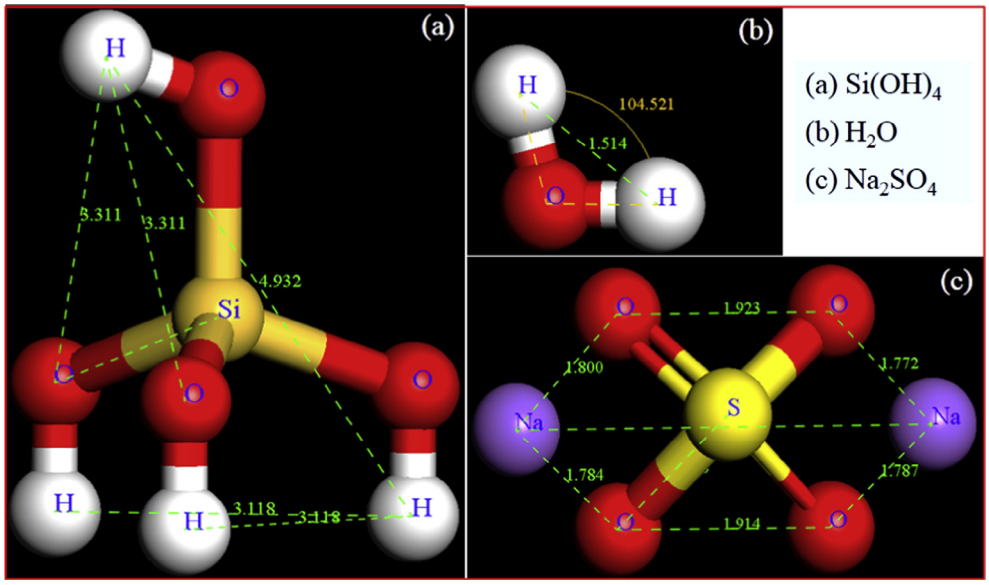

Fig. 2. Structures and properties of molecules in the studied reaction and aggregation process. The red, gold, white, purple and yellow beads represent oxygen, silicon, hydrogen, sodium and sulfur atoms, respectively. (For interpretation of the references to colour in this figure legend, the reader is referred to the web version of this article.)

Table 1
Properties of molecules in the initial simulation box after geometry optimization step.

Parameter	Element		
	$Si(OH)_4$	Na_2SO_4	H_2O
Bond lengths (Å)	Si—O, +1.90 O—H, +1.11	S—O, +1.50 Na—O, +1.78 O—O, +1.92	O—H, +0.99 O—O, +1.51
Diameter (Å)	4.90	3.74	1.51
Partial charge (eV)	Si, +0.89 O, −0.47 H, +0.25	Na, +1.00 S, +1.51 O, −0.88	O, −0.82 H, +0.41

of the final configurations was 1 g/cm^3. The silicic acid, sodium sulfate and water molecules with 4.9, 3.7 and 1.5 Å in diameter were distributed randomly in the simulation box. The prepared cubic simulation box was followed by a relaxation process to achieve minimum energy structures. A snapshot of the periodic initial simulation system can be seen in Fig. 3. The structure of the initial system demonstrated that there were numerous unfilled spaces in the simulation box. The silicic acid, sodium sulfate, and water molecules were distributed non-uniformly. The geometry optimization step was done to find the equilibrium structures of the mentioned molecules, eliminate unfilled spaces and make the molecule distribution more uniform, where no reaction occurs during the time of optimization.

3.2. MD simulation details and protocol

All MD calculations were conducted using the Materials Studio (MS) software which has already been successfully used to explore aggregation phenomenon (Gholizadeh and Yu, 2014). The dreiding force field of MS package was used in the whole calculation to search for all bonding, angle, dihedral, and inversion potential sets for a given configuration (Chang and Violi, 2006). This force field is applicable for simulation of biological, organic and main-group inorganic molecules to determine structures and dynamics (Mayo et al., 1990). Dreiding force field is established to use general force constants and geometry parameters. This application applies through simple hybridization considerations rather than individual force constants and geometric parameters that depend on the particular combination of atoms involved in the bond, angle, or torsion terms. In regards to this definition, bond distances are derived from atomic radii and there is one force constant for each bond, angles, and inversions and six different values for torsional barriers. The mentioned factors are defined for all possible combinations of atoms. The total potential energy of the simulation system depends on the Cartesian coordinates of the atoms and contains contributions from intramolecular (bonded) interactions and intermolecular (non-bonded) interactions. The potential energy of dreiding force fields contains additive terms for a quadratic bond stretching potential, a quadratic angle bending potential, a trigonometric torsion potential, a quadratic out-of-plane potential, Coulomb interactions, van der Waals interactions, and hydrogen bonds. The energy function is described in the following equation (6):

$$U(\overrightarrow{R}) = \sum_{\text{bonds}} K_b(b-b_0)^2 + \sum_{\text{UB}} K_{UB}(S-S_0)^2 + \sum_{\text{angle}} K_\theta(\theta-\theta_0)^2 + \sum_{\text{dihedrals}} K_\chi(1+\cos(n\chi-\delta)) + \sum_{\text{impropers}} K_{imp}(\phi-\phi_0)^2 + \sum_{\text{nonbound}} \varepsilon\left(\left(\frac{R_{min_{ij}}}{r_{ij}}\right)^{12} - 2\left(\frac{R_{min_{ij}}}{r_{ij}}\right)^{6}\right) + \frac{q_i q_j}{\varepsilon_l r_{ij}} \quad (6)$$

where K_b, K_{UB}, K_θ, K_χ, and K_{imp} are the bond, Urey–Bradley, angle, dihedral angle, and improper dihedral angle force constants, respectively. b, S, θ, χ, and ϕ are the bond length, Urey–Bradley 1,3-distance, bond angle, dihedral angle, and improper torsion angle, respectively. The subscript zero represents the equilibrium values for the individual terms. Coulomb and Lennard–Jones 6–12 terms contribute to the external or non-bonded interactions; ε is the Lennard–Jones well depth and R_{min} is the distance at the Lennard–Jones minimum; q_i is the partial atomic charge; ε_l is the effective dielectric constant; and r_{ij} is the distance between atoms i and j. Given $\overrightarrow{R}$, the vector of the coordinates of the atoms, the various distances and angles required to evaluate $U(\overrightarrow{R})$ in Eq. (6) are easily determined. All possible bond angles and dihedral angles are included in $U(\overrightarrow{R})$, while a limited number of Urey–Bradley terms and improper

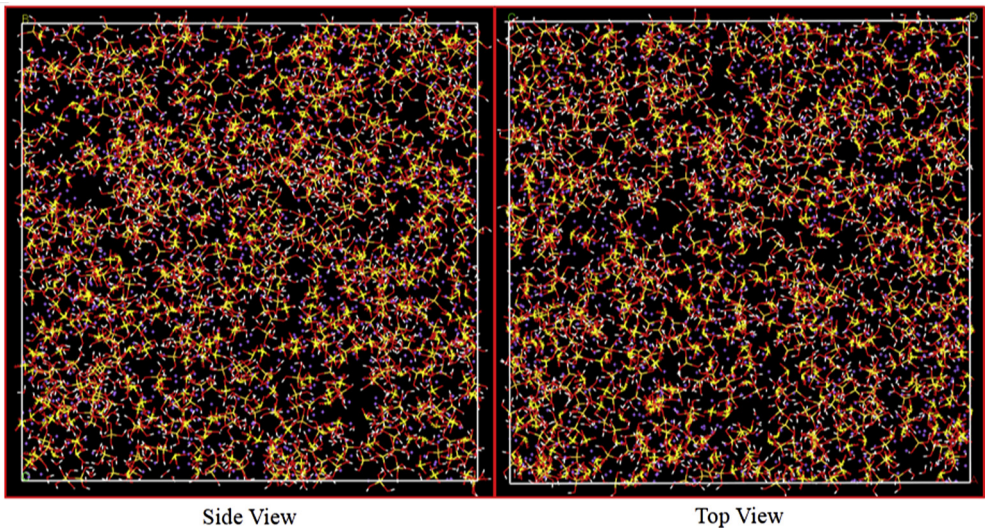

Fig. 3. Snapshots of the initial simulation system. The colors scheme is the same as that used in Fig. 2. (For interpretation of the references to colour in this figure legend, the reader is referred to the web version of this article.)

dihedral angles are used to optimize the fit to vibrational spectra. The van der Waals part of the non–bond interaction is modeled using the Lennard–Jones *n-m* potential (LJ^{n-m}, $n = 12$, and $m = 6$) function for the Born repulsion and vdW attraction terms, respectively, and a Coulombic potential function for the electrostatic interaction (Sun, 1998)

$$E_{ij} = \sum_{i,j} \frac{q_i q_j}{r_{ij}} + \sum_{i,j} \varepsilon_{ij} \left[\frac{m}{n-m} \left(\frac{\sigma_{ij}}{r_{ij}} \right)^n - \frac{n}{n-m} \left(\frac{\sigma_{ij}}{r_{ij}} \right)^m \right] \tag{7}$$

where q_i, q_j and r_{ij} are the charges and the distance between atoms i and j, respectively. ε is the potential well depth for the interactions between atoms and σ_{ij} is the collision diameter of atoms i and j at which the potential becomes zero. For a pair of dissimilar atoms, σ_{ij} in Eq. (8), where the σ_i and σ_j values of the individual atoms are based on the Waldman–Hagler combination rule (Waldman and Hagler, 1993):

$$\sigma_{ij} = \left[\frac{(\sigma_i)^6 + (\sigma_j)^6}{2} \right]^{1/6} \tag{8}$$

The ε_{ij} value is presented by

$$\varepsilon_{ij} = 2\sqrt{\varepsilon_i \varepsilon_j} \left(\frac{\sigma_i^3 \sigma_j^3}{\sigma_i^6 + \sigma_j^6} \right) \tag{9}$$

The values of σ_i, σ_j, ε_i and ε_j for silicon and oxygen atoms are 4.45 Å, 3.30 Å, 0.198 kcal/mol and 0.080 kcal/mol, respectively (Bergström, 1997; Sun, 1998). Therefore, the calculated σ and ε values using Eqs. (8) and (9) for Si and O atom interactions are σ_{Si-O} = 4.07 Å and ε_{Si-O} = 0.088 kcal/mol, respectively. Furthermore, the Hamaker constant is measured to be about 9.49 kcal/mol, which is consistent with the experimental value of 9.35–12.75 kcal/mol, given by Bergstrom (Bergström, 1997). ($A_H = \pi^2 C/v^2$, where $C = 3\varepsilon_{Si\text{-}O}\ \sigma^6_{Si-O}$ is the vdW attraction interaction parameter and $v = 4/3\pi(\sigma_{Si-O}/2)^3$ is the atom volume of about 35.3 Å^3).

Minimization step of the initial simulation boxes was performed using the smart minimizer approach followed by the conjugate gradient (Fletcher–Reeves) method. The maximum iterations and quality of convergence in minimization step were 1000 and fine respectively. The MD simulations were carried out in the canonical NVT ensemble at an initial temperature of 343.15 K for 4000 ps with the step size of 1 fs, which allows the stress of the system to change under the external load in the whole simulation. Our simulations were conducted for a much longer period of time, compared with other studies (Alimohammadi and Fichthorn, 2009; Mustan et al., 2015). The Andersen thermostat was used for maintaining the constant temperature with a fictitious mass, Q, ratio of 1.0. Newton's equations of motion were integrated using the velocity Verlet algorithm with a time step of 1 fs (1.0×10^{-15} s) (Andrea et al., 1983). Periodic boundary conditions were applied in all three directions, and the electrostatic interactions were calculated using the particle mesh Ewald method with a tolerance of 10^{-4} (D'Angelo et al., 2015). The cutoff distance of the L–J potential was chosen to be 6.00 Å with cubic spline truncation. The temperature in all the simulations was equilibrated with the Velocity scale algorithm (Andrea et al., 1983). The atom-based cutoffs were used with the explicit atom sums being calculated to 4.50 Å. The tail correction was applied to non–bonded interactions during the MD run. All parameters such as force field type, thermodynamic ensemble, target temperature and dynamics time are determined in terms of simulation conditions of desired chemical reaction.

4. Results and discussion

The results of the simulations are described in three sections. First, parameters such as number and size of aggregates and pores are calculated. Furthermore, the shape of aggregates, "volume of pores" and the effect of variations of reactants' numbers on "diameters and numbers" of "aggregates and pores" investigated is discussed. Second, few thermodynamic properties such as Gibbs free energy, enthalpy, and entropy of aggregation are obtained from the simulations. Third, it is shown that the studied colloidal solution is unstable (aggregation occurred) according to the achieved results of Gibbs free energy calculations and molecular dynamics simulations including mean squared displacements (MSD), radial distribution functions (RDF), evaluations of aggregation conditions. It is necessary to mention that the word "pore" in this article implies the distances between aggregates.

4.1. Aggregation of silicic acid monomers in the simulation box

The shape of the aggregates can be determined from the description of the principal moments of inertia. The three principal moments of inertia, λ_1, λ_2, and λ_3 are obtained from the eigenvalues

of the matrix of the radii of gyration of the aggregates. The matrix of the radii of gyration is explained by the following equation (10):

$$R^2_{x^\alpha x^{\alpha'}} = \frac{1}{q}\sum_{p=1}^{q}(x_p^\alpha - x_{cm}^\alpha)(x_p^{\alpha'} - x_{cm}^{\alpha'}) \quad (10)$$

where α and α' can take values of 1, 2, or 3 corresponding to the three Cartesian coordinates, which represents the coordinate of a site p (in the aggregate) in the α direction, the subscript cm stands for the center of mass, and q is the total number of sites occupied by the aggregate. The characteristic length is defined as $\Gamma_\alpha = (\lambda_\alpha)^{0.5}$. A measure of the aggregate sphericity can be obtained from the calculation of Γ_1/Γ_3 and Γ_2/Γ_3 as functions of the aggregate size. For a spherical aggregate Γ_1/Γ_3 and $\Gamma_2/\Gamma_3 = 1$, and for a cylindrical one, $\Gamma 1/\Gamma_3 \gg 1$ and $\Gamma_2/\Gamma_3 = 1$ (Rodríguez-Guadarrama et al., 1999). An aggregate is defined as an assembly which is composed of two or more silicon atoms and the aggregate size is the number of silicon atoms it included. It is found that the shapes of the aggregates were approximately spherical given the geometrical constraints of the cubic lattice in the simulations. Furthermore, the shapes of the aggregates were explored using visualization of a simulation box.

A snapshot of the simulation box and one of a randomly selected aggregate are shown in Fig. 4. This figure demonstrates that the shapes of aggregates are approximately spherical. The structures of created aggregates in the simulation box are a reminder of the diverse aggregation models. The sizes of aggregates were determined directly using the measurement of distances tool from the Sketch toolbar in MS. Diameters and numbers of aggregates and pores were determined and are presented in Fig. 5. The size of aggregates continuously increased from 1 nm to 2.5 nm while the number of aggregates had a dissimilar behavior. First, the number of aggregates increased from 4 to 7 and then decreased to 3. Continuously, silicic acid particles grow larger before aggregation and gelling occur, and such a long period leads to a close packed microstructure with a large particle size, generating silica nanomaterial and ultimately aggregation of silica nanoparticles takes place. Gelling occurs when about half of the silica has entered the gel phase, which can be thought of as spherical solidified regions in suspension which cause a rapid increase in viscosity when the volume fraction reaches about 0.5. Related information about size and number of created aggregates in the simulation box are presented in Table 2. Visually, the aggregates appear to be dense by the aggregation of some smaller spheroid aggregates. The predominant aggregate diameter is 2 nm which is 33% of the simulation box lattice parameter. Similarly, the size of pores increased from 0.5 nm to 2 nm while their number had different behavior. The number of pores increased from 8 to 12 and then decreased to 7. In addition, firstly the pore volumes increased and then decreased. Summarized information about size, number, and volume of produced pores in the simulation box are presented

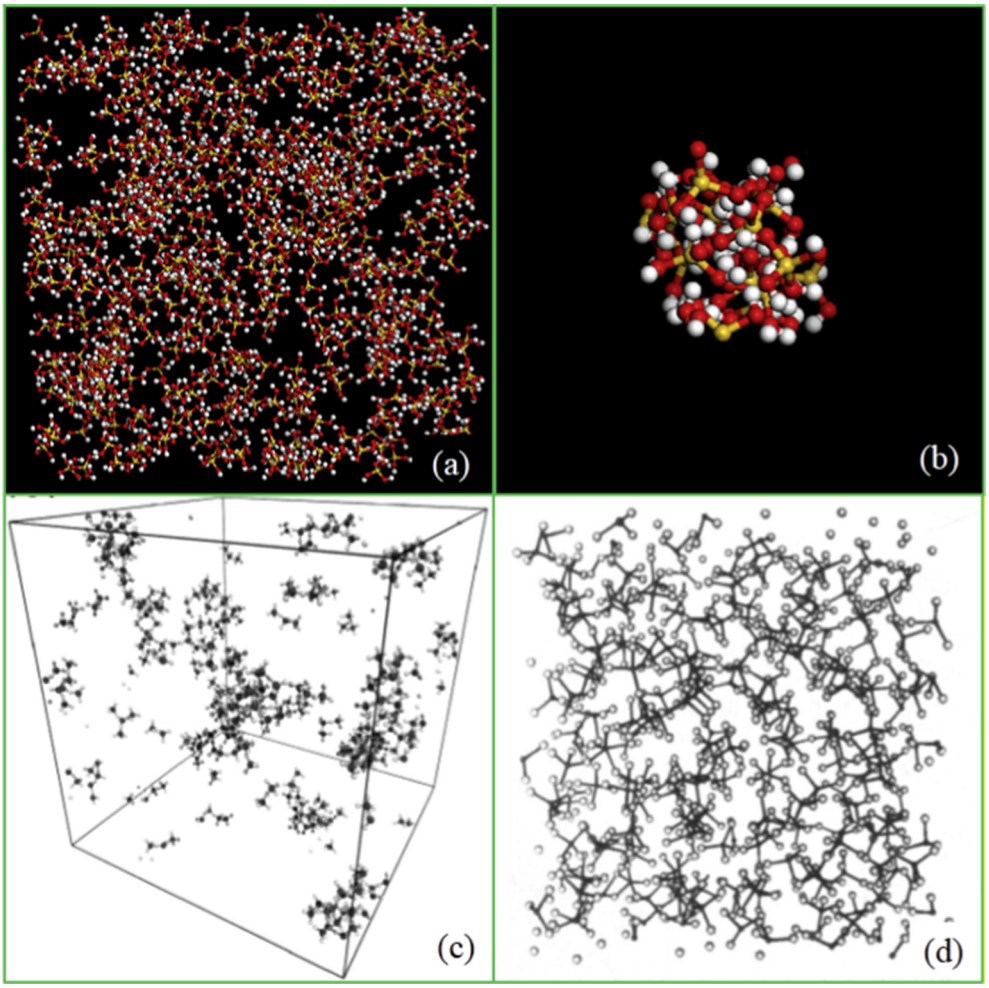

Fig. 4. (a) Aggregation of silicic acid monomers in (this study) (b) randomly selected spherical aggregate in the simulation box after MD simulations (this study) (c) A snapshot of $Si(OH)_4$ aggregation from implemented simulation by Rao et al. (d) Snapshot of the aggregation of H_4Si0_4 molecules system by Garofalini, S.H. et al. Only SiO bonds are shown in the snapshot; H ions are not drawn in the figure.

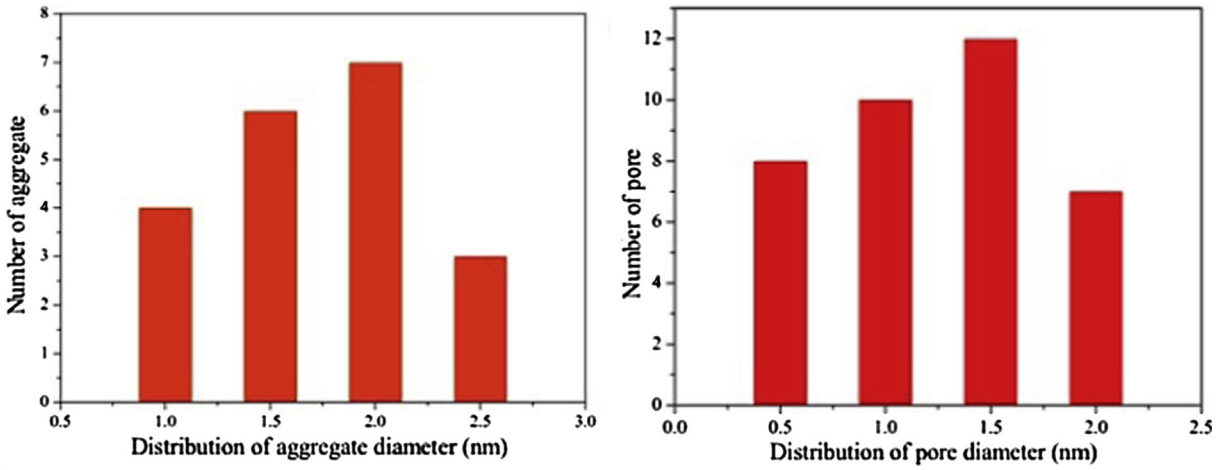

Fig. 5. Distributions of the aggregates and pores' diameters in the simulation box (time steps, 1 fs). The y-axis represents aggregate numbers (a) and pore numbers (b).

Table 2
Specifications of produced aggregates and pores during the aggregation process.

Number (N_{agg}) and Diameter of Aggregates (D_{agg})	Number (N_P) and Diameter of Pores (D_p)	Pore Volume (nm^3)
4, ~1 nm	8, ~0.5 nm	~0.07
6, ~1.5 nm	10, ~1 nm	~0.53
7, ~2 nm	12, ~1.5 nm	~1.77
3, ~2.5 nm	7, ~2 nm	~4.19

in Table 2. Our simulation results illustrate that the aggregates and pores with 2 nm and 1.5 nm in size were predominant in the simulation box when the primary particle size of silicic acid monomer was 0.49 nm. The fluctuations of obtained values of diameter, number, and volume of aggregates and pores were in agreement with other theoretical and experimental investigations (Garofalini and Martin, 1994; Rao and Gelb, 2004; Zhang et al., 2016). Specifications such as size, volume, distribution, and topology of pores have a crucial role on adsorption, transport phenomena or aggregation processes (Ban, 2009). Rao et al. conducted a research on molecular dynamics simulations of the polymerization of aqueous silicic acid and the analysis of the effects of concentration on silica polymorph distributions, growth mechanisms, and reaction kinetics (Rao and Gelb, 2004). They found that the conversion of monomers to dimers and addition of monomers to small clusters takes place at the initial steps of the polymerization process while at longer times cluster–cluster aggregation is observed. In addition, Fig. 4 shows a snapshot of $Si(OH)_4$ aggregation process from implemented simulation by Rao and Gelb (2004) (Fig. 4c). Their initial configuration for simulation was constructed by distributing 729$Si(OH)_4$ molecules in a (9 Å × 9 Å × 9 Å) simple cubic array. The final density of simulation system was 1.0 g/cm^3 and the initial configuration was allowed to relax at 300 K for 10 ps. Furthermore, Garofalini, S.H. et al., theoretically investigated the aggregation of silicic acid molecules and network formation (Fig. 4d). 216 H_4Si0_4, silicic acid molecules, (1944 ions) had been studied using the molecular dynamics computer simulation technique. Densities varied from 1.4 to 1.6 g/cm^3 and the time step was $l0^{-4}$ ps (Garofalini and Martin, 1994). With the comparison of our implemented simulations and other researchers (see Fig. 4), it is revealed that there is a good compatibility between sizes of aggregates and pores, and volumes of pores of theoretical results in this research and other studies.

Beside the studied simulation box in the beginning parts of this article, two simulation boxes constructed using the amorphous cell module to determine the relationship between "diameters and numbers" of "aggregates and pores" with the variations of reactants' numbers were used. These simulation boxes included 3000 molecules (1000$Si(OH)_4$, 1000 Na_2SO_4 and 1000 H_2O) and 4500 molecules (1500$Si(OH)_4$, 1500 Na_2SO_4 and 1500 H_2O) which were different numbers of effective molecules on the aggregation process. These systems are named as box 1 (1500 molecules), box 2 (3000 molecules) and box 3 (4500 molecules), respectively. MD simulation parameters for these systems implemented according to mentioned method and values in Section 4.2. Although, the lattice parameters of these three studied simulation boxes obtained 60 Å × 60 Å × 60 Å, 75 Å × 75 Å × 75 Å, and 86 Å × 86 Å × 86 Å, respectively, the variations of "numbers and diameters" of "aggregates and pores" were remarkable and considerable. The number of aggregates increased while their diameters slightly decreased when the number of effective molecules on the aggregation process increased. The average diameter of aggregates was about 1.5–2 nm and distributed uniformly in the simulation boxes. Similarly, the number of pores increased while their diameters slightly decreased when the number of reactants increased. The predominant diameter of pores was about 2 nm although three relatively large pores observed in the simulation box of 3000 molecules (1000$Si(OH)_4$, 1000 Na_2SO_4 and 1000 H_2O). The volume of pores in the simulation boxes roughly decreased except the mentioned large pores. Further research could explore the effect of different pH on the aggregation process can be very valuable. It is clear that higher values of pH lead to more OH^- in the solution which means that they cooperate to create bonds to aggregate particles. Therefore, fluctuations of pH influence diameters and distributions of aggregates and pores. Higher values of OH^- ions increase the velocity of polymerization reaction. Subsequently, the primary particles grow dramatically in diameter when they are aggregated into the network.

4.2. Thermodynamic parameters from the simulations

Improving the knowledge through thermodynamic analysis on the aggregation behavior of silicic acid monomer helps researchers to have more insights of the driving forces and molecular details involved in the aggregation processes. Thermodynamic analysis implemented via Gibbs energy, enthalpy, and entropy of aggregate formation. For a given concentration of molecules and dimensionless interaction energy, the size distribution of the aggregates obtained from the simulations can be used directly to calculate the Gibbs free energy of aggregation using Eq. (11) as follows (Rodríguez-Guadarrama et al., 1999),

$$\frac{\Delta G_n^{\circ}}{k_B T} = \ln X_1 - \frac{1}{n}\ln X_n \tag{11}$$

where k_B, T, ΔG_n°, n are the Boltzmann constant, temperature, standard Gibbs free energy of aggregation, aggregation number, respectively. X_1 and X_n are the mole fractions of a single mono–silicic acid and aggregates of size n. $\Delta G_n^{\circ} = (\mu_n^{\circ}/n) - \mu_1^{\circ}$ is the difference in the standard Gibbs free energy between an mono–silicic acid molecule in an aggregate of size n and a free mono-silicic acid in the colloidal solution. The standard chemical potentials are represented by μ_n° for an aggregate of size n, by μ_0° for the colloidal solution, and by μ_1° for a single mono-silicic acid molecule. If $\frac{\Delta G_n^{\circ}}{k_B T}$ is calculated for a range of interaction energies, the standard enthalpy of aggregation $\frac{\Delta H_n^{\circ}}{k_B T}$ can be determined at any $\varepsilon^*/k_B T$ within the range from the Gibbs–Helmholtz equation (12)

$$\left.\frac{\Delta H_n^{\circ}}{k_B T}\right|_{\varepsilon^*/k_B T} = \left.\frac{d\left(\frac{\Delta G_n^{\circ}}{k_B T}\right)}{d\ln(\varepsilon/k_B T)}\right|_{\varepsilon^*/k_B T} \tag{12}$$

Then the entropy of aggregation ΔS_n° follows from

$$\Delta G = \Delta H - T\Delta S \tag{13}$$

Calculation of Gibbs energy determines the reaction proceeding (spontaneous, equilibrium, nonspontaneous) and stability or instability (aggregation process) of a colloidal solution. Bai et al. have studied the thermodynamic parameters for the aggregation process in aqueous solutions (Acton, 2012; Bai et al., 2008). Their research demonstrated that the large negative values of the Gibbs free energy (G) are primarily due to an entropic contribution. In colloidal solutions, if free energy has a negative value, this indicates aggregation takes place and the reaction is spontaneous (favored reaction), but if free energy has a positive value this indicates stable solution and the reaction is nonspontaneous (disfavored reaction). In addition, particles collide randomly via Brownian motions to reduce surface areas through attaching together. Gibbs free energy is calculated from obtained values of simulations for entropy, enthalpy, and temperature. Furthermore, we have calculated the entropy of aggregation by the method described above using the size distribution data obtained from the simulations. In addition, particles collide randomly via Brownian motions to reduce surface areas by attaching together. Standard enthalpy, entropy and Gibbs energy values of involved molecules in the aggregation process are presented in Table 3 (Haynes, 2012; Sefcik and Goddard, 2001).

According to the Eqs. (11)–(13) and Table 3, the standard Gibbs energy, enthalpy and entropy of aggregation were calculated to be −211.3, −214.7 kJ/mol and −9.8 J/mol K, respectively, at 343.15 °K. The negative Gibbs energy confirms that aggregation occurred during the production of silica materials via precipitation method. The obtained values for thermodynamic functions were in agreement with other researchers' measurements (Rodríguez-Guadarrama et al., 1999). These values indicate that association of silicic acid monomers occurred, spontaneously. The large negative values of the Gibbs energy are primarily due to an entropic contribution, an effect common in aggregation processes driven by hydrophobicity.

4.3. RDF and MSD analyses

Radial distribution function (RDF) plays a key role in the statistical mechanics of simulation systems which contain particles such as atoms, molecules, and colloids. RDF describes how the atoms are radially packed around each other in a solution (Kirkwood and Boggs, 1942). The RDF is defined by Hansen and McDonald (1986):

$$x_\alpha x_\beta \rho g_{\alpha\beta}(r) = \frac{1}{N}\left\langle \sum_{i=1}^{N_\alpha}\sum_{i=1}^{N_\beta}\delta(r - r_i + r_j)\right\rangle \tag{14}$$

where x_i and N_i are the mole fraction and the number of atoms of chemical type I, respectively. N is the total number of atoms and ρ is the overall number density. The MD trajectory information from NVT simulations is used to calculate intermolecular radial distribution functions (RDF). In this research, RDF is evaluated to determine the changed densities of H_2O and Na_2SO_4 molecules around silicic acid molecules in the simulation box. Fig. 6a shows the RDF for the $Si(OH)_4$—Na_2SO_4&H_2O molecules in the colloidal solution (simulation system). There are five peaks under 4 Å but two major peaks at short distances (under 3.8 Å) at 0.9 and 1.6 Å are considered because of their importance as the geometric center of silicic acid monomer was selected as the mapping center. The first sharp RDF peak around 1 Å indicate the covalent OH bonds. The second RDF peak around 1.8 Å indicates the hydrogen from the proton donating water, which means the oxygen of the OH has an incomplete tetrahedral structure. In the former cases, the first peak corresponds to a face–on motif, and the second peak a side–on motif. Similar structural features had been observed in other researchers studied systems. The dynamic characteristic calculation of molecules and atoms in a simulation system such as colloidal solutions is one of the well-known computable parameters of MD simulations. The mean squared displacement (MSD) is determined based on the position of the particle over time. The mean squared displacement of the particles with respect to their original position is related to the diffusion coefficient (Lu et al., 2015),

$$D = \frac{1}{6}\lim_{t\to\infty}\frac{d}{dt}\sum_{i=1}^{N_a}|r_i(t) - r_i(0)|^2 \tag{15}$$

where r_i denotes the position vector of i_{th} particle, and the angular brackets denote an ensemble average. The slope of the MSD curve as a function of time is proportional to the diffusion coefficient of the diffusing atoms. Displacement of atoms and molecules is related to particle mobility and the big displacement increment demonstrates stronger activity. Therefore, the change of silicic acid particles activity is achievable through recording the variations of MSD curve slopes during the simulation processes (Im et al., 2016). Total MSD curve of involved molecules in the aggregation process is presented in Fig. 6b. Fig. 6b shows the diffusion of the species included in the simulation. A graph for all species is presented in this figure. All silicon, oxygen and hydrogen atoms of silicic acid monomers nanoparticles were considered for preparing of MSD curve. The activity of silicic acid particles is proportional to the slopes of MSD curve. High at the beginning of simulation decreasing slowly during the simulation. The activity decreased at the end of simula-

Table 3
Standard thermodynamic properties of molecules involved in aggregation process (Acton, 2012; Sefcik and Goddard, 2001).

Parameter	Molecule				
	H_2O	SiO_2	Na_2SO_4	H_2SO_4	Na_2SiO_3
Entropy (J/mol K)	+69.90	+41.5	+149.60	+156.9	+113.9
Enthalpy (kJ/mol)	−285.8	−910.7	−1387.1	−814.0	−1554.9
Gibbs free Energy (kJ/mol)	−237.1	−856.7	−1270.2	−689.9	−1462.8

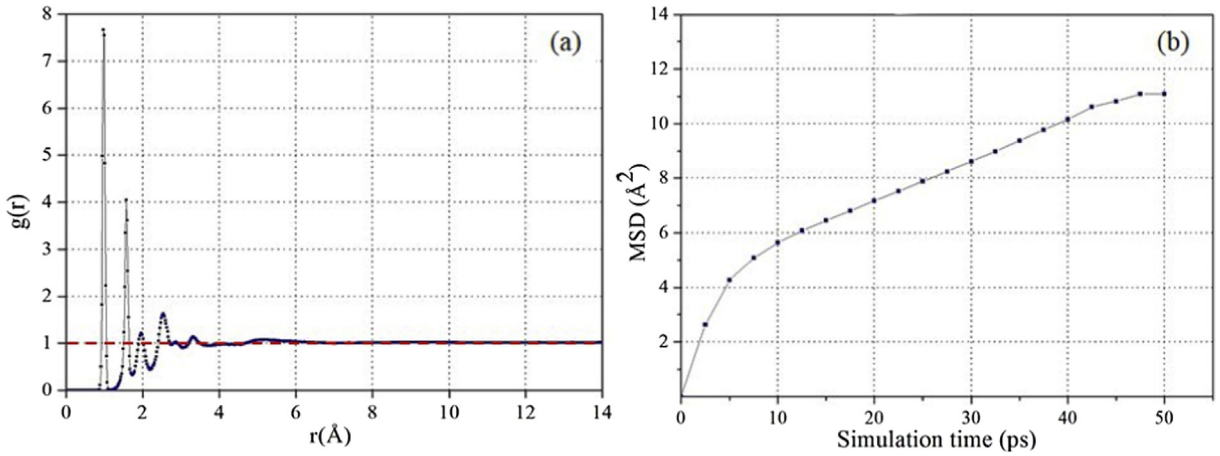

Fig. 6. (a) RDF and (b) MSD curves of silicic acid monomers nanoparticles and other molecules in the simulation system.

tion demonstrates that silicic acid monomers came toward each other to produce larger particles and aggregation occurred.

5. Conclusions

The main objective of this study was modeling of the aggregation process of silicic acid monomers in the colloidal solution using MD simulations. The lack of knowledge about mechanisms of formed aggregates and structures during the molecular simulations encouraged us to implement this research. Aggregation phenomenon occurs in the late steps of silica materials production through the precipitation method, while the stability takes place in the early stages for an extended period time. Several investigations of aggregation process carried out by other researchers based on a hypothesis, which was applying an external energy on the silica nanoparticles. This hypothesis could not illustrate different types of interaction forces among different kinds of particles and molecules in a real colloidal solution. The determined thermodynamic parameters of studied colloidal solution from the results of MD simulations reveal that the aggregation phenomenon occurred during the production of silica materials. Parameters such as atoms distribution (RDF), the position of the particles over time (MSD), diameters and numbers of aggregates and pores, and volumes of pores were calculated from the results of MD simulations. Aggregates and pores diameters increased whereas the number of aggregates and pores first increased and then decreased. Furthermore, the volume of pores first increased and then decreased. Variations of reactants' numbers had remarkable influences on the pores and aggregates topologies. The number of aggregates and pores increased while their diameters slightly decreased when the numbers of effective molecules on the aggregation process increased. The next step is to repeat the calculations using the Mesocite module from MS package and compare it with the current study. The Mesocite module is more accurate and implements an extensive range of classical mechanics calculations using classical force–field based simulation techniques. In addition, Mesocite DPD carries out simulations using any force–field and groups of molecules, called dissipative particles, that are considered instead of fluid molecules.

Acknowledgement

This work was financially supported by the National Basic Research Foundation of China (Grant 2013CB733600) and the National Natural Science Foundation (Grants 21276140, 20976096, and 21036002).

Notes

The authors declare no competing financial interests.

References

Acton, Q.A., 2012. Solvents: Advances in Research and Application: 2011 Edition: ScholarlyBrief. Scholarly Editions.

Alimohammadi, M., Fichthorn, K.A., 2009. Molecular dynamics simulation of the aggregation of titanium dioxide nanocrystals: preferential alignment. Nano Lett. 9, 4198–4203. https://doi.org/10.1021/nl9024215.

Andrea, T.A., Swope, W.C., Andersen, H.C., 1983. The role of long ranged forces in determining the structure and properties of liquid water. J. Chem. Phys. 79, 4576.

Aydin, F., Chu, X., Uppaladadium, G., Devore, D., Goyal, R., Murthy, N.S., Zhang, Z., Kohn, J., Dutt, M., 2016. Self-assembly and critical aggregation concentration measurements of ABA triblock copolymers with varying B block types: model development, prediction, and validation. J. Phys. Chem. B 120, 3666–3676. https://doi.org/10.1021/acs.jpcb.5b12594.

Bai, G., Lopes, A., Bastos, M., 2008. Thermodynamics of micellization of alkylimidazolium surfactants in aqueous solution. J. Chem. Thermodyn. 40, 1509. https://doi.org/10.1016/j.jct.2008.05.016.

Ban, S., 2009. Computer Simulation of Zeolites: Adsorption, Diffusion and Dealumination door. Utrecht University Repository.

Bergström, L., 1997. Hamaker constants of inorganic materials. Adv. Colloid Interface Sci. 70, 125–169. https://doi.org/10.1016/S0001-8686(97)00003-1.

Chang, R., Violi, A., 2006. Insights into the effect of combustion-generated carbon nanoparticles on biological membranes: a computer simulation study. J. Phys. Chem. B 110, 5073–5083. https://doi.org/10.1021/jp0565148.

Chou, H.C., Chiu, S.J., Liu, Y.L., Hu, T.M., 2014. Direct formation of S-nitroso silica nanoparticles from a single silica source. Langmuir 30, 812–822. https://doi.org/10.1021/la4048215.

D'Angelo, P., Serva, A., Aquilanti, G., Pascarelli, S., Migliorati, V., 2015. Structural properties and aggregation behavior of 1-Hexyl-3-methylimidazolium Iodide in aqueous solutions. J. Phys. Chem. B 119, 14515–14526. https://doi.org/10.1021/acs.jpcb.5b08739.

Delay, M., Frimmel, F.H., 2012. Nanoparticles in aquatic systems. Anal. Bioanal. Chem. 402, 583–592. https://doi.org/10.1007/s00216-011-5443-z.

Du, L., Tan, J., Wang, K., Lu, Y., Luo, G., 2011. Controllable preparation of SiO_2 nanoparticles using a microfiltration membrane dispersion microreactor. Ind. Eng. Chem. Res. 50, 8536–8541. https://doi.org/10.1021/ie2003363.

Dzyaloshinskii, I.E., Lifshitz, E.M., Pitaevskii, L.P., 1961. General theory of van der Waals' forces. Sov. Phys. Uspekhi 4, 153.

Garofalini, S.H., Martin, G., 1994. Molecular simulations of the polymerization of silicic acid molecules and network formation. J. Phys. Chem. 98, 1311–1316. https://doi.org/10.1021/j100055a044.

Gholizadeh, R., Yu, Y.-X., 2014. Work functions of pristine and heteroatom-doped graphenes under different external electric fields: an ab initio DFT study. J. Phys. Chem. C 118.

Giannini, V., Fernández-Domínguez, A.I., Heck, S.C., Maier, S.A., 2011. Plasmonic nanoantennas: fundamentals and their use in controlling the radiative properties of nanoemitters. Chem. Rev. 111, 3888–3912. https://doi.org/10.1021/cr1002672.

Gompper, G., Ihle, T., Kroll, D.M., Winkler, R.G., 2012. Multi-particle collision dynamics: a particle-based mesoscale simulation approach to the hydrodynamics of complex fluids. Adv. Comput. Simul. Approaches Soft Matter Sci. III, 1–34. https://doi.org/10.1007/12.

Grzelczak, M., Vermant, J., Furst, E.M., Liz-Marzán, L.M., 2010. Directed self-assembly of nanoparticles. ACS Nano 4, 3591–3605. https://doi.org/10.1021/nn100869j.

Guo, X., Zhang, L., Qian, Y., Zhou, J., 2007. Effect of composition on the formation of poly (dl-lactide) microspheres for drug delivery systems: mesoscale simulations. Chem. Eng. J. 131, 195–201. https://doi.org/10.1016/j.cej.2007.01.013.

Hamaker, H.C., 1937. The London-van der Waals attraction between spherical particles. Physica 4, 1058–1072. https://doi.org/10.1016/S0031-8914(37)80203-7.

Haynes, W.M., 2012. CRC Handbook of Chemistry and Physics. Taylor & Francis. CRC Handbook of Chemistry and Physics.

He, Y., Ma, K., Bi, L., Feng, J.Y., Zhang, Z.J., 2006. Nickel-induced enhancement of photoluminescence from Si-rich silica films. Appl. Phys. Lett. 88, 31905. https://doi.org/10.1063/1.2165292.

Hoang, V. Van, 2007. Molecular dynamics simulation of amorphous SiO_2 nanoparticles. J. Phys. Chem. B 111, 12649–12656. https://doi.org/10.1021/jp074237u.

Hu, B., Cao, X., Zhang, P., 2013. Selective colorimetric detection of glutathione based on quasi-stable gold nanoparticles assembly. New J. Chem. 37, 3853–3856. https://doi.org/10.1039/C3NJ00978E.

Hu, B., Wang, S.B., Wang, K., Zhang, M., Yu, S.H., 2008. Microwave-assisted rapid facile "Green" synthesis of uniform silver nanoparticles: self-assembly into multilayered films and their optical properties. J. Phys. Chem. C 112, 11169–11174. https://doi.org/10.1021/jp801267j.

Hunter, R.J., 1987. Foundations of Colloid Science. Oxford University Press, New York.

Iler, R.K., 1979. The Chemistry of Silica: Solubility, Polymerization, Colloid and Surface Properties and Biochemistry of Silica. Wiley.

Im, S., Kim, H., Maeng, J., Yu, J., Cha, Y., Paeng, S.-H., 2016. On the mean square displacement of a random walk on a graph. Eur. J. Comb. 51, 227–235. https://doi.org/10.1016/j.ejc.2015.05.009.

Hansen, J.P., McDonald, I.R., 1986. Theory of Simple Liquids. second ed., Academic Press.

Jenkins, S., Kirk, S.R., Persson, M., Carlen, J., Abbas, Z., 2009. Molecular dynamics simulation of nanocolloidal amorphous silica particles: part III. J. Chem. Phys. 130, 134702. https://doi.org/10.1063/1.3102957.

Jenkins, S., Kirk, S.R., Persson, M., Carlen, J., Abbas, Z., 2008. Molecular dynamics simulation of nanocolloidal amorphous silica particles: Part II. J. Chem. Phys. 128. https://doi.org/10.1063/1.2906462.

Jurkić, L.M., Cepanec, I., Pavelić, S.K., Pavelić, K., 2013. Biological and therapeutic effects of ortho-silicic acid and some ortho-silicic acid-releasing compounds: new perspectives for therapy. Nutr. Metab. (Lond) 10 (2). https://doi.org/10.1186/1743-7075-10-2.

Kim, T., Lee, C., Joo, S., Lee, K., 2008. Kinetics of gold nanoparticle aggregation: experiments and modeling. J. Colloid Interface Sci. 318, 238–243.

Kirk, S.R., Yin, D., Persson, M., Carlen, J., Jenkins, S., 2011. Molecular dynamics simulations of the aggregation of nanocolloidal amorphous silica monomers and dimmers. Procedia Eng. 18, 188–193. https://doi.org/10.1016/j.proeng.2011.11.030.

Kirkwood, J.G., Boggs, E.M., 1942. The radial distribution function in liquids. J. Chem. Phys. 10.

Li, X., Lenhart, J.J., Walker, H.W., 2012. Aggregation kinetics and dissolution of coated silver nanoparticles. Langmuir 28, 1095–1104. https://doi.org/10.1021/la202328n.

Li, X., Lenhart, J.J., Walker, H.W., 2010. Dissolution-accompanied aggregation kinetics of silver nanoparticles. Langmuir 26, 16690–16698. https://doi.org/10.1021/la101768n.

Lu, J., Liu, D., Yang, X., Zhao, Y., Liu, H., Tang, H., Cui, F., 2015. Molecular dynamics simulations of interfacial interactions between small nanoparticles during diffusion-limited aggregation. Appl. Surf. Sci. 357, 1114–1121. https://doi.org/10.1016/j.apsusc.2015.09.142.

Mayo, S.L., Olafson, B.D., Goddard, W.A.I., 1990. DREIDING: A generic force field for molecular simulations. J. Phys. Chem. 101, 8897–8909. https://doi.org/10.1021/j100389a010.

Milling, A., Mulvaney, P., Larson, I., 1996. Direct measurement of repulsive van der waals interactions using an atomic force microscope. J. Colloid Interface Sci. 180, 460–465. https://doi.org/10.1006/jcis.1996.0326.

Mustan, F., Ivanova, A., Madjarova, G., Tcholakova, S., Denkov, N., 2015. Molecular dynamics simulation of the aggregation patterns in aqueous solutions of bile salts at physiological conditions. J. Phys. Chem. B 119, 15631–15643. https://doi.org/10.1021/acs.jpcb.5b07063.

Ogorzalek, T.L., Wei, S., Liu, Y., Wang, Q., Brooks, C.L., Chen, Z., Marsh, E.N.G., 2015. Molecular-level insights into orientation-dependent changes in the thermal stability of enzymes covalently immobilized on surfaces. Langmuir 31, 6145–6153. https://doi.org/10.1021/acs.langmuir.5b01735.

Pashley, R., 1981. DLVO and hydration forces between mica surfaces in Li^+, Na^+, K^+, and Cs^+ electrolyte solutions: a correlation of double-layer and hydration forces with surface cation exchange properties. J. Colloid Interface Sci. 83, 531–546. https://doi.org/10.1016/0021-9797(81)90348-9.

Patel, A.C., Li, S., Wang, C., Zhang, W., Wei, Y., 2007. Electrospinning of porous silica nanofibers containing silver nanoparticles for catalytic applications. Chem. Mater. 19, 1231–1238. https://doi.org/10.1021/cm061331z.

Pereira, J.C.G., Catlow, C.R.A., Price, G.D., 1999. Ab initio studies of silica-based clusters. Part II. Structures and energies of complex clusters. J. Phys. Chem. A 103, 3268–3284. https://doi.org/10.1021/jp982867d.

Pereira, J.C.G., Catlow, C.R.A., Price, G.D., Almeida, R.M., 1997. Atomistic modeling of silica based sol-gel processes. J. Sol-Gel Sci. Technol. 8, 55–58. https://doi.org/10.1023/A:1026434701722.

Pereira, J.C.G., Catlow, C.R.A., Pereira, C.G.J., Price, G.D., 1998. Silica condensation reaction: an ab initio study. Chem. Commun., 1387–1388 https://doi.org/10.1039/A801816B.

Rao, N.Z., Gelb, L.D., 2004. Molecular dynamics simulations of the polymerization of aqueous silicic acid and analysis of the effects of concentration on silica polymorph distributions, growth mechanisms, and reaction kinetics. J. Phys. Chem. B 108, 12418–12428. https://doi.org/10.1021/jp049169f.

Rodríguez-Guadarrama, L.a., Talsania, S.K., Mohanty, K.K., Rajagopalan, R., 1999. Thermodynamics of aggregation of amphiphiles in solution from lattice Monte Carlo simulations. Langmuir 15, 437–446. https://doi.org/10.1021/la9806597.

Schiller, P., Krüger, S., Wahab, M., Mögel, H.J., 2011. Interactions between spheroidal colloidal particles. Langmuir 27, 10429–10437. https://doi.org/10.1021/la2015918.

Sefcik, J., Goddard, W.A., 2001. Thermochemistry of silicic acid deprotonation: Comparison of gas-phase and solvated DFT calculations to experiment. Geochim. Cosmochim. Acta 65, 4435–4443. https://doi.org/10.1016/S0016-7037(01)00739-6.

Sharma, M., Trout, B.L., 2015. Effect of pore size and interactions on paracetamol aggregation in porous polyethylene glycol diacrylate polymers. J. Phys. Chem. B 119, 8135–8145. https://doi.org/10.1021/jp512788a.

Sun, H., 1998. COMPASS: an ab initio force-field optimized for condensed-phase applicationsoverview with details on alkane and benzene compounds. J. Phys. Chem. B 102, 7338–7364. https://doi.org/10.1021/jp980939v.

Sun, H., Rigby, D., 1997. Polysiloxanes: ab initio force field and structural, conformational and thermophysical properties. Spectrochim. Acta Part A Mol. Biomol. Spectrosc. 53, 1301–1323. https://doi.org/10.1016/S1386-1425(97)00013-9.

Sun, W., Zeng, Q., Yu, A., 2013a. Calculation of noncontact contact forces between silica nanospheres. Langmuir 29, 7825–7837. https://doi.org/10.1021/la401087j.

Sun, W., Zeng, Q., Yu, A., Kendall, K., 2013b. Calculation of normal contact forces between silica nanospheres. Langmuir 29, 7825–7837. https://doi.org/10.1021/la401087j.

Vold, M.J., 1982. Zeta potential in colloid science. Principles and applications. J. Colloid Interface Sci. 88, 608. https://doi.org/10.1016/0021-9797(82)90296-X.

Waldman, M., Hagler, A.T., 1993. New combining rules for rare gas van der waals parameters. J. Comput. Chem. 14, 1077–1084. https://doi.org/10.1002/jcc.540140909.

Wang, J., Zhang, F., Wang, Y., Luo, G., Cai, W., 2016. A size-controllable preparation method for indium tin oxide particles using a membrane dispersion micromixer. Chem. Eng. J. 293, 1–8. https://doi.org/10.1016/j.cej.2016.02.053.

Wang, Y., Zhang, C., Bi, S., Luo, G., 2010. Preparation of ZnO nanoparticles using the direct precipitation method in a membrane dispersion micro-structured reactor. Powder Technol. 202, 130–136. https://doi.org/10.1016/j.powtec.2010.04.027.

Yamahara, K., Okazaki, K., 1998. Molecular dynamics simulation of the structural development in sol–gel process for silica systems. Fluid Phase Equilib. 144, 449–459. https://doi.org/10.1016/S0378-3812(97)00289-6.

Yang, Y., Matsubara, S., Nogami, M., Shi, J., 2007. Controlling the aggregation behavior of gold nanoparticle. Mater. Sci. Eng., B 140, 172–176.

Yu, Y.-X., 2014. Binding energy and work function of organic electrode materials phenanthraquinone, pyromellitic dianhydride and their derivatives adsorbed on graphene. ACS Appl. Mater. Interfaces 6, 16267–16275. https://doi.org/10.1021/am504452a.

Zhang, T., Wang, Y., Luo, G., Bai, S., 2016. Effects of precipitation and drying processes on the synthesis of silica materials with a large-pore-volume and narrow-pore-diameter distribution. Ind. Eng. Chem. Res. 55, 3579–3587. https://doi.org/10.1021/acs.iecr.5b03641.